Received May 9, 2020, accepted May 27, 2020, date of publication June 1, 2020, date of current version June 12, 2020.

Digital Object Identifier 10.1109/ACCESS.2020.2998835

A Novel High-Gain Sum and Difference Conical Beam-Scanning Reflector Antenna

JUNXIANG YANG, (Student Member, IEEE), SHI-SHAN QI, (Member, IEEE), WEN WU, (Senior Member, IEEE), AND DA-GANG FANG, (Life Fellow, IEEE)
School of Electronic and Optical Engineering, Nanjing University of Science and Technology, Nanjing 210094, China

Corresponding author: Shi-Shan Qi (qishishan@gmail.com)

This work was supported in part by the National Natural Science Foundation of China under Grant 61771242.

ABSTRACT A novel sum and difference (SD) conical beam-scanning reflector antenna is proposed in this paper. The reflector surface, illuminated by two omnidirectional horns, is a body of revolution obtained by revolving the generating parabola about a symmetry axis. The horns stacked along the symmetry axis of the reflector are fed by a nest coaxial waveguide. Teflon lens is used to improve the side lobe levels and reflection coefficients of the feed horns. By tilting the generating parabola and using the offset feeding method, two conical beams, with different beam pointing angles, were generated. A compact feed network was also designed to feed the two horns, which includes two rectangular TE_{10} mode-to-coaxial TEM mode transitions and a Magic-T to implement SD beams. The scanning performance of conical beams can be achieved by mechanically moving the feed antennas along the symmetry axis and taking full advantage of offset focus characteristic of the parabolic reflector. The error in angle measurement was also discussed. The SD conical beam-scanning antenna was formed by a parabolic dish with a radius of 18 λ operating at 24 GHz. The proposed antenna was designed, simulated, and fabricated. The measured results show that the difference beam null-depth is -25 dB and the sum beam gain is 15 dBi at 40°. The sum beam gain varies by less than 1.5 dB across the scan coverage from 30.8° to 45.2°. The measured results are found to be in good agreement with the simulated ones.

INDEX TERMS Reflector antenna, conical beam, magic-T, sum and difference beams.

I. INTRODUCTION

Of late, much attention has been paid to conical beam antennas, because they are good candidates for satellite communication, target detection, tracking or guiding system, and so on. Conical beam antennas are superior to phased array antennas and omnidirectional antennas in TACAN-tactical air navigation system, vehicles communication, etc., because of their low cost and better performance. Satcom on the Move (SOTM) system needs high-gain and wide-beam coverage to obtain good quality communication [1]. The conical beam-scanning antennas with sum and difference beams for tracking capability can give better performance-to-cost ratio.

Different from the traditional pencil beam monopulse antennas [2]–[4], the beam coverage of conical beam antenna is a ring area rather than a spot area. Therefore, conical beam antennas have intrinsic advantage of being wide beam coverage that is very important in many applications. Consequently, unlike the pencil beam the gain reaches 15dBi with 40° beam-pointing angle will be considered to be high gain. Conical beam patch antennas are reported to be switchable between a broadside and a conical radiating mode by exciting different modes of the radiator [5]–[9]. A hybrid topology optimization method, for designing an LP and CP conical-beam patch antennas, is proposed in [10]. Circularly polarized antennas with conical beam radiation patterns are introduced in [11], in which the feed networks are very simple, with no need for power divider. Slot antennas with conical-beam radiation are described in [12], whose angle of maximum gain depends on the tilt angle of the cone. In [13], [14], reconfigurable conical beam-pointing angle antennas with variable frequencies are reported. In [15], [16], nested horn antenna is proposed to produce conical beams with different beam-pointing angles by controlling the diameters of coaxial waveguide horn and circular waveguide horn. A helmet antenna with conical beams, based on artificial magnetic conductors, is presented in [17], which is wearable and compact.

The associate editor coordinating the review of this manuscript and approving it for publication was Davide Ramaccia.

In the above-cited references, the conical beam antennas are with either low-gain or small beam-pointing angle. To improve the gain of the conical beam antennas, three kinds of antennas are used: lens antenna, array antenna, and reflector antenna. The dielectric lens, used in high-gain conical beam antennas, is usually very large and bulky [18]. Array antenna proposed in [19]–[23] suffers from complex feeding network, complicated structure, high profile, and difficulty in beam-scanning. Reflector antennas, with single and dual reflectors, have been investigated for single high-gain conical beam [24]–[27].

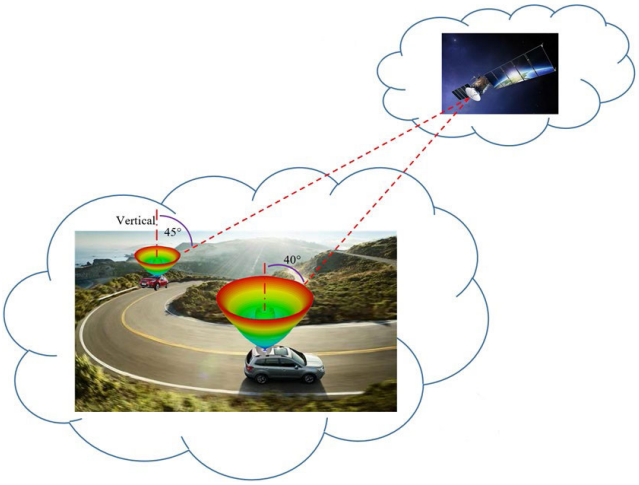

FIGURE 1. Application diagram of a conical beam-scanning reflector antenna mounted on vehicles moving on the earth that is communicating with a Navigation Satellite.

In practical SOTM systems, conical beam-scanning antenna with high-gain and wide-beam coverage is desirable because of the relevant movement between the antenna and the satellite. The operation bandwidth of the STOM is too narrow to form a frequency-scanning conical beam. Conical beams have wide-beam coverage in azimuth plane. And tracking of the satellite in the elevation plane can be realized by sum and difference conical beams, as shown in Fig. 1. Therefore, conical beam-scanning characteristic of a fixed frequency is a good choice for SOTM. An omnidirectional dual reflector antenna is proposed in [26] for flexible coverage. It provides scanning conical beam by moving the sub-reflector along the common symmetry axis of the dual-reflector. However, it lacks the capability of tracking, which is required for a high signal-to-noise ratio. To obtain the tracking capability in the SOTM system, the SD beams are introduced, which produce an error needed for tracking [28]. In addition, because of the rotational symmetric feature, the conical beams can only realize one-dimensional tracking.

In this paper, a SD conical beam-scanning reflector antenna, with the capability of tracking the beam-pointing angle, is proposed. Rotational symmetric reflecting surface, with parabolic generating curve, was illuminated by two primary omnidirectional horns (see Fig.2). By tilting the generating parabolic curve and using the offset feeding method, two conical beams, with different beam pointing angles, could be generated. To suppress the higher-order modes of the coaxial waveguide with large radius, four-way ridge waveguides have been used to feed the outer nested feeding horn. The inner horn was fed by a simple rectangular-to-coaxial waveguide transition. In addition, a comparator network was also designed to coordinate with the horns and reflecting surface and to produce the high-gain SD conical beams. SD conical beams-scanning performance was realized by mechanically moving the total feed along the symmetry axis and taking full advantage of offset focus characteristic of the parabolic reflector. Thus, a reflector antenna with a radius of 18 λ was designed, fabricated, and tested. The measured gain of the sum conical beam, with 40° beam-pointing angle, was 15 dBi, whereas the null depth of the difference conical beams could reach −25 dB at 24 GHz. Moving the feed horns along the symmetry axis allowed the sum conical beam to be scanned from 30.8° to 45.2°. This structure can make full use of the antenna aperture to obtain higher aperture efficiency and is easy to fabricate at K band.

II. GEOMETRY OF THE PROPOSED ANTENNA

The proposed antenna is composed of two nested omnidirectional horns and a reflector, and both of them are bodies of revolution with a common symmetry axis (the z axis), as depicted in Fig. 2. Wa is the width of the antenna conical aperture and D_{M} is the diameter of the reflector outer rim. The architecture of the feed of SD conical beam antenna is illustrated in Fig. 3.

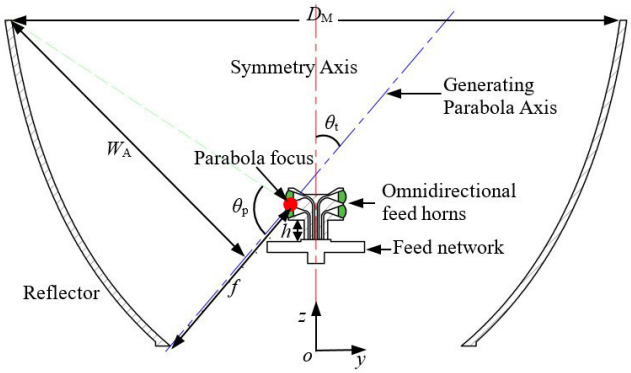

FIGURE 2. Cross-sectional view of the proposed SD conical beam-scanning reflector antenna.

Feed network and omnidirectional feed horns are shown in Fig. 4. To produce a set of parallel omnidirectional beams, two horns are stacked along the z axis and fed by nested coaxial waveguide 1 and 2. The inner and outer radii of the coaxial waveguide 1 and the coaxial waveguide 2 are r_1, r_2, r_3, r_4, respectively. Teflon lenses ($\varepsilon_{\mathrm{r}} = 2.1$, and $\tan\delta = 0.001$) were placed at the apertures of the horns to improve the impedance matching and decrease the side lobe levels. Outer contours of the Teflon lens were generated by parabolas. The focuses O_1 and O_2 of the parabolas were placed at the phase center

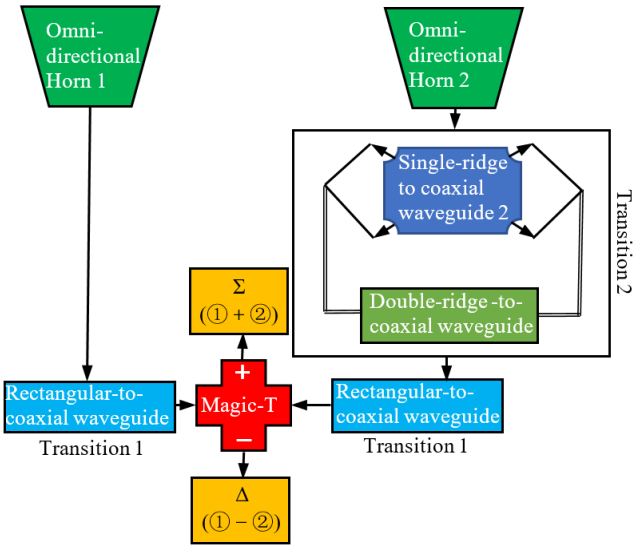

FIGURE 3. Block diagram of designing the feed of SD conical beam antenna.

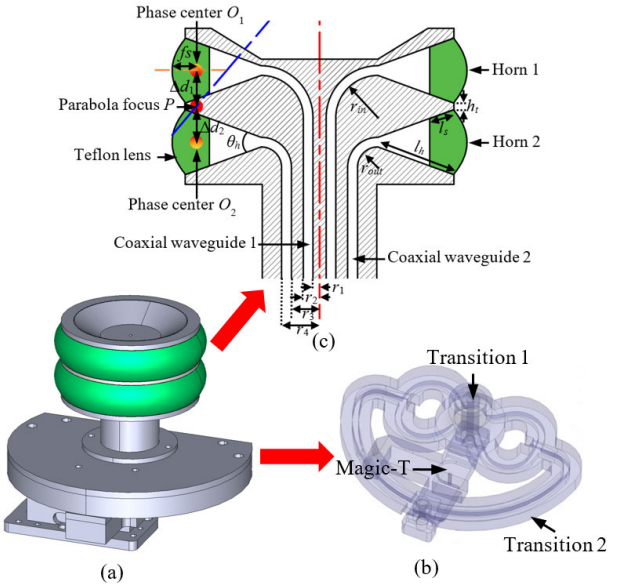

FIGURE 4. Configuration of the feed. (a) Feed of the antenna. (b) Inside view of the feed network. (c) Cross-sectional view of the omnidirectional feed horns.

of the horns, which were calculated by HFSS. The focus P of the reflector was set at the center of O_1 and O_2. The traces of P, O_1, and O_2, spanning 360° around z axis, form three ring. The focal length of the reflector is f. The primary radiation pattern of each feed horn was determined from the requirement of the −7-dB edge illumination and the details are given in Section III. Optimized dimensions of the relevant parameters in this design are listed in Table 1.

Fig. 5 shows the structure of the magic-T and transition 1 of the rectangular-to-coaxial waveguide 1. The comparator network is stemmed by a traditional waveguide magic-T. For large impedance ratio between rectangular and coaxial waveguides and good return loss performance over a wide frequency band [29], a 4-section Chebyshev impedance

TABLE 1. Dimensions of the proposed antenna and the feed horns (length: mm and angle: °).

Parameter	Value	Parameter	Value	Parameter	Value
D_M	459	W_A	250	θ_t	40
θ_p	84	f	140	h	20
r_1	1	r_2	2.5	r_3	4.35
r_4	5.85	r_{in}	6.5	r_{out}	3.15
h_t	1	l_h	12.5	l_s	4
fs	3	θ_h	40	Δd_1	5.5
Δd_2	5.5				

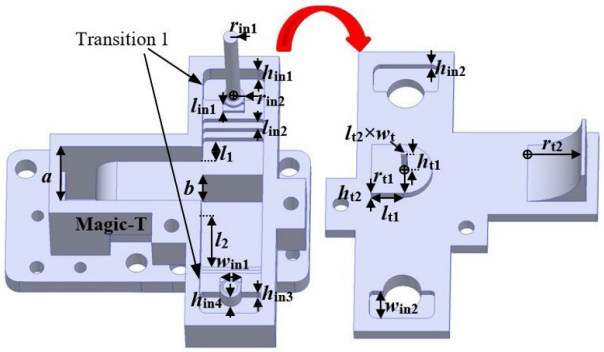

FIGURE 5. Magic-T and rectangle-to-coaxial waveguide 1.

transformer was used in the matching transition. Optimized dimensions of the relevant parameters in this design are listed in Table 2.

TABLE 2. Dimensions of the magic-t and transition 1 (length: mm).

Parameter	Value	Parameter	Value	Parameter	Value
a	8.636	b	4.318	l_{t1}	4.318
l_{t2}	0.75	r_{t1}	3.75	r_{t2}	7.32
h_{t1}	1.2	h_{t2}	4.5	w_t	0.5
l_1	6.7	l_2	4.4	l_{in1}	1
l_{in2}	1	h_{in1}	3	h_{in2}	1
h_{in3}	1.53	h_{in4}	2.63	r_{in1}	1
r_{in2}	1.5	w_{in1}	3	w_{in2}	4.2

Fig. 6 shows the configuration of the coaxial-to-coaxial waveguide 2, that is, transition 2, which is a heart-like structure. For good return loss performance over a wide frequency band, arc trace connection between the single-ridge rectangular waveguide and Port 4 was used [30]. Moreover, four parallel 200-Ω single-ridge rectangular waveguides were utilized to maintain the circular symmetry of the electromagnetic field required for excitation of pure TEM mode in the coaxial waveguide 2. In addition, two parallel 100-Ω double-ridge rectangular waveguides were used to connect the 50-Ω coaxial waveguide and 200-Ω single-ridge waveguide. Optimized dimensions of the relevant parameters in this design are presented in Table 3.

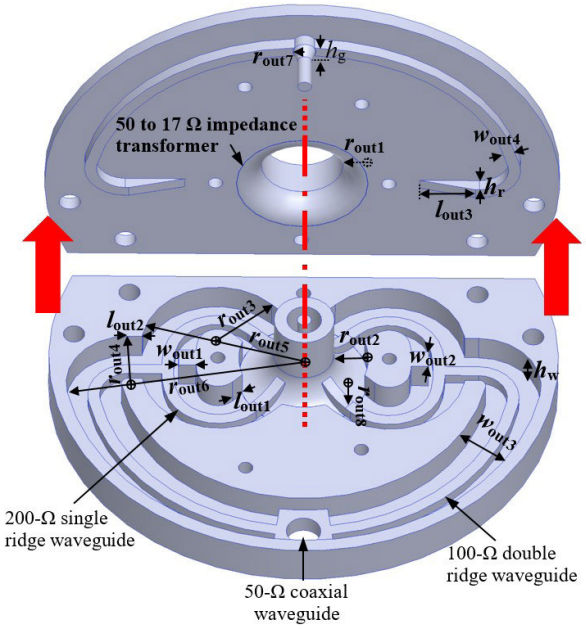

FIGURE 6. Configuration of the transition 2.

TABLE 3. Dimensions of the transition 2 (length: mm).

Parameter	Value	Parameter	Value	Parameter	Value
r_{out1}	3.5	r_{out2}	5	r_{out3}	11
r_{out4}	9	r_{out5}	23.6	r_{out6}	34.7
r_{out7}	1.6	r_{out8}	7.45	w_{out1}	2.5
w_{out2}	2.8	w_{out3}	8	w_{out4}	1.7
h_g	1.8	h_r	1.7	h_w	4.3

III. ANALYSIS OF THE PROPOSED ANTENNA

This section introduces the analysis of the feed network and design of the reflector. The proposed structures were analyzed using HFSS and CST.

A. ANALYSIS OF THE FEED NETWORK AND THE HORNS

Magic-T is an important component of the feed network, which is used for the sum and difference outputs. To obtain SD characteristics, the difference-signal between Port 03 and Port 04 is excited at Port Δ while the sum-signal is obtained at Port Σ. Ports 03, 04, and Σ form the H-arm T-junction of the magic-T. Similarly, Ports 03, 04, and Δ constitute the E-arm T-junction of the magic-T. The process can also be viewed from the E-field distribution in magic-T shown in Fig. 7.

Fig. 8 (a) shows the coaxial-to-rectangular waveguide transition 1. It has been observed that electromagnetic waves are transmitted mainly in TEM mode between the coaxial waveguide and the up wall of the ridged waveguide, and then radiate into the multistep impedance transformer, with just a little energy being propagated into the short-circuited waveguide cavity.

The ratio of the external radius to the inner radius of the coaxial waveguide 2 is smaller than the corresponding ratio

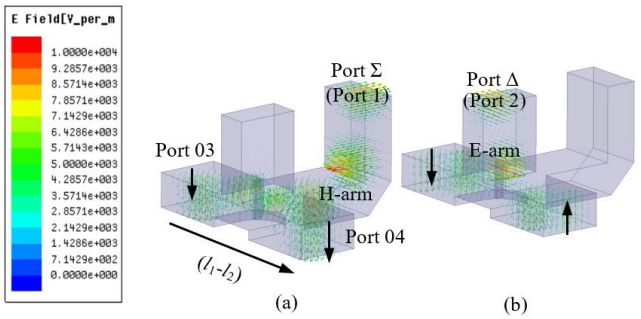

FIGURE 7. E-field distributions at 24 GHz in Magic-T: (a) Port Σ is excited; (b) Port Δ is excited.

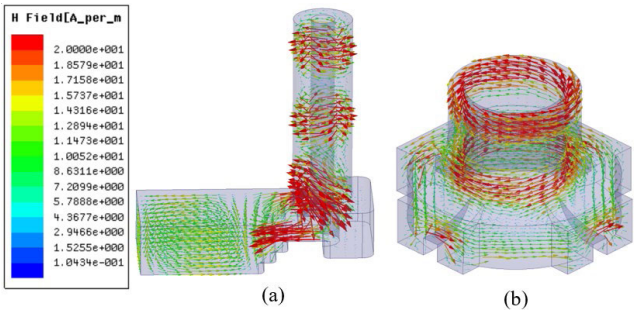

FIGURE 8. H-field distribution at 24 GHz in rectangular-to-coaxial waveguide transition. (a) Transition 1. (b) Impedance transformer.

in the coaxial waveguide 1 because of the external position (r_4:r_3 < r_2:r_1). The widths between the inner and the outer conductors of the two nested coaxial waveguides should be the same to produce two similar patterns required from the illumination ($r_2 - r_1 = r_4 - r_3$). As a result, the characteristic impedance of coaxial waveguide 2 is only 17 Ω, which is much smaller than that of the coaxial waveguide 1. Simultaneously, the higher-order modes of the coaxial waveguide 2 will appear. To solve these problems, a 50 to 17 Ω continuously tapered coaxial waveguide impedance transformer was used, as shown in Fig. 8 (b).

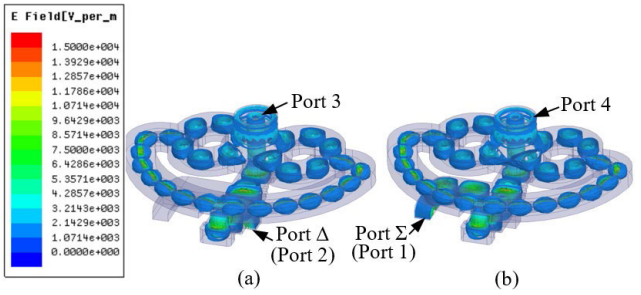

FIGURE 9. E-field distributions at 24 GHz in the feed network: (a) Port Σ is excited; (b) Port Δ is excited.

Fig. 9 plots the E-field distribution in the feed network and four ports in the feed network. It can be found that pure TEM mode in the coaxial waveguides 1 and 2 are obtained. S-parameters of the Port 1, Port 2, Port 3 and Port 4 are plotted

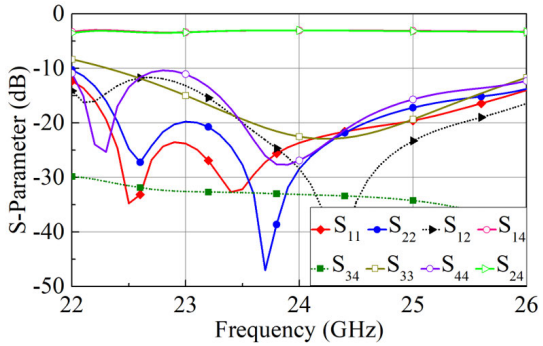

FIGURE 10. Simulated S-parameters of the feed network ($l_1 - l_2 = 2.3$mm).

in Fig. 10. It can be found that Port 1 and Port 2 are well isolated at 24 GHz, as well as Port 3 and Port 4. The results are quite satisfactory in consideration of multiple reflections from different parts of the network. The phase deviation of the corresponding ports in the in-phase comparison and the out-of-phase comparison both are less than 5.0°.

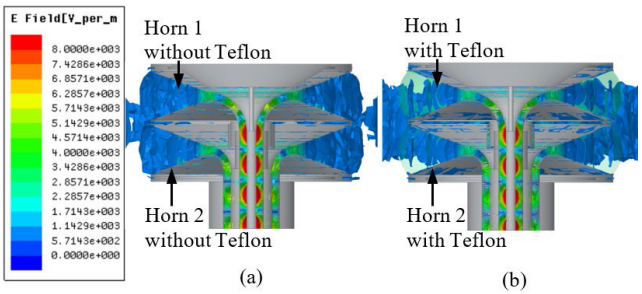

FIGURE 11. E-field distributions in the omnidirectional feed horns. (a) Without lens. (b) With lens.

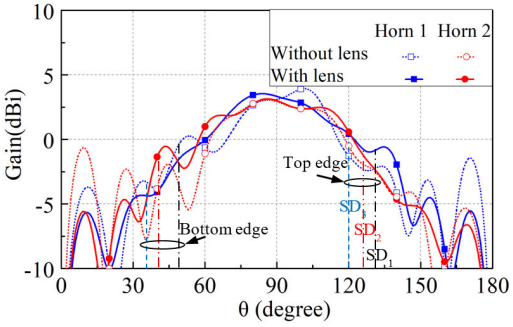

FIGURE 12. Simulated *yoz* cut radiation patterns of the feed antennas, with and without lens (only half is shown because of the symmetry).

The omnidirectional feed horns can be uniquely determined once the θ_h and l_h are given. $\theta_h = 40°$ and $l_h = \lambda$ are obtained based on [31]. Teflon lens was introduced to improve impedance matching. Fig. 11 shows E-field distributions in the omnidirectional feed horns with and without Teflon lens. The simulation results of these two cases are shown in Fig. 12 and Fig. 13. In comparison, the omnidirectional horns with Teflon lens not only exhibit more uniform

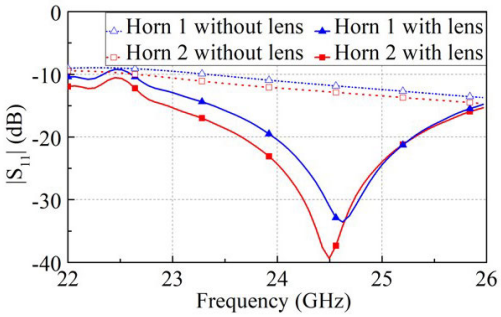

FIGURE 13. Simulated reflection coefficients of the feed horn.

illumination to the reflector from 48° to 132° but also feature lower lobes near z axis (see Fig. 12). In addition, the reflection coefficients improved significantly by adding Teflon lens (see Fig. 13), as described in [32]. It indicates that Teflon lens plays the role of phase adjustment and impedance matching.

B. DESIGN OF THE REFLECTOR

The contour curve of the reflector is generated by the left half of the parabola. Analysis of this axially symmetric reflector was carried out based on [24]–[27], [33]–[38]. The location of the focal point P can be determined by the phase center of the two nested feed horns as shown in Fig. 4. θ_p is dependent on the beam width of the nested feed antennas. From the previous discussion in Section 2, the generating curve can be uniquely determined once the θ_t, W_A, and f parameters are given. θ_t is specified beam pointing angle, W_A is determined from the required gain, and f is calculated from θ_p and W_A.

The auxiliary $y_r P z_r$ coordinate system is defined by rotating and offsetting the yoz coordinate system, with its origin at the parabolic focus, as follows:

$$\begin{bmatrix} y_r \\ z_r \end{bmatrix} = \begin{bmatrix} \cos\theta_t & -\sin\theta_t \\ \sin\theta_t & \cos\theta_t \end{bmatrix} \begin{bmatrix} y \\ z \end{bmatrix} + \begin{bmatrix} y_P \\ z_P \end{bmatrix} \tag{1}$$

where y_P, z_P are the y and z coordinates of the aperture focus point P in the yoz coordinate system. The auxiliary coordinate system and some pertinent geometric parameters are illustrated in Fig. 14.

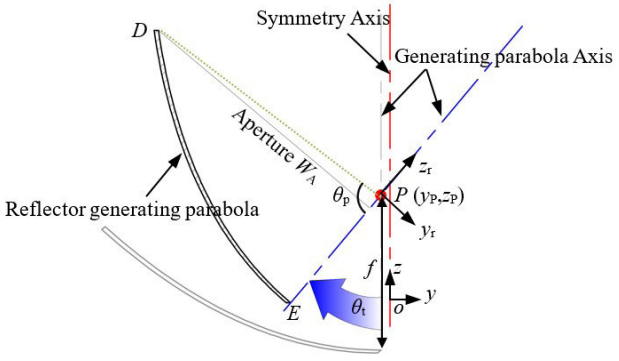

FIGURE 14. Basic parameters of the reflector generating parabola.

Assuming a uniform field distribution over the reflector's aperture, the maximum directivity D_0 at θ_t is given

approximately by the following formula [25]:

$$D_0 \approx \frac{2W_A}{\lambda \sin\theta_t} \tag{2}$$

This equation is valid for main-beam tilts at least 30° from the vertical in this paper.

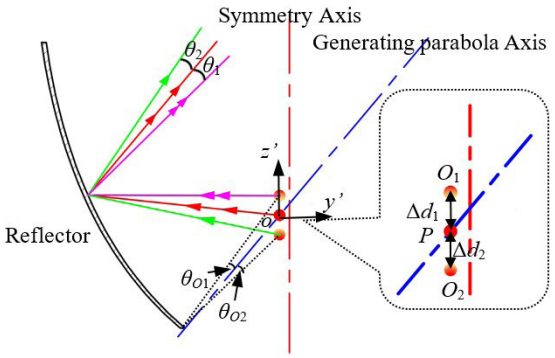

FIGURE 15. Displacement of the feed horns. When the feed of a parabolic reflector antenna is displaced laterally from the focal point, the beam is shifted off-axis in the opposite direction to the feed displacement.

When the feed of a parabolic reflector antenna is displaced laterally from the focal point, the beam shifts off-axis in the opposite direction [33]–[37]. As a result, two conical beams can be obtained by placing the two feed horns on both sides of the focus of the reflector, as shown in Fig. 15. θ_{O1} and θ_{O2} denote the angular displacements of the feed horns, and θ_1, θ_2 the beam pointing angles of the two conical beams. Given that Δd is much less than f, the beam deviation factor (BDF) can be obtained by the following equation [38]:

$$\text{BDF}=\frac{\theta_1}{\theta_{O1}}=\frac{\theta_2}{\theta_{O2}}=\frac{1+\kappa(W_A/4f)^2}{1+(W_A/4f)^2} \tag{3}$$

where $\kappa = 0.5027$ is the scale coefficient, whereas the values of f and W_A can be taken from Table 1. Thus, it is established that BDF=0.9177. θ_1, θ_2 can be calculated as follows:

$$\begin{aligned}\theta_1 &= 0.9177 \times \theta_{O1}\\ \theta_2 &= 0.9177 \times \theta_{O2}\end{aligned} \tag{4}$$

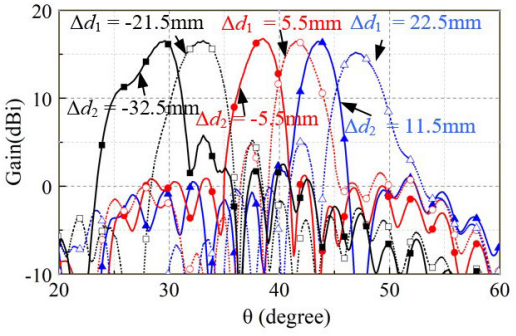

FIGURE 16. Simulated yoz cut radiation patterns of the conical beam reflector antenna, with different values of Δd, $\theta_t = 40°$ (only half is shown because of the symmetry).

Fig. 16 shows the simulated radiation patterns, obtained by displacing two single horns along the z' axis separately.

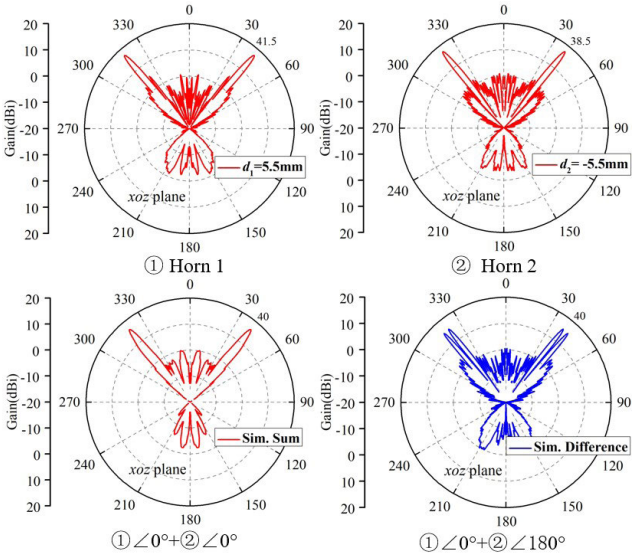

FIGURE 17. Illustration of the synthesis of sum and difference conical patterns, obtained by the superposition of two conical beams ($\theta_t = 40°$).

It can be seen that, by moving the feed antennas along the z' axis, the beam pointing angle can be continuously changed. Fig. 17 depicts the synthesis of sum and difference conical beams, obtained by the superposition of two conical beams. It can be found that a sum conical beam (Σ) forms by adding the two conical beams (in phase), and a difference conical beam (Δ) forms by subtracting the two corresponding conical beams (out phase). The difference in propagation path between coaxial waveguide 1 and coaxial waveguide 2 leads to an additional phase difference in the aperture of the horn 1 and horn 2. To compensate the corresponding phase difference, initial phase required at the output of the feed network should be adjusted by tuning the lengths of two co-linear arms of the magic-T (l_1, l_2). Two omnidirectional horns produce two primary patterns, which are reflected by the reflection surface, and generate two high-gain conical beams. Sum and difference conical beams are obtained by the superposition of two conical beams through magic-T. Simulated 3-D radiation patterns are shown in Fig. 18.

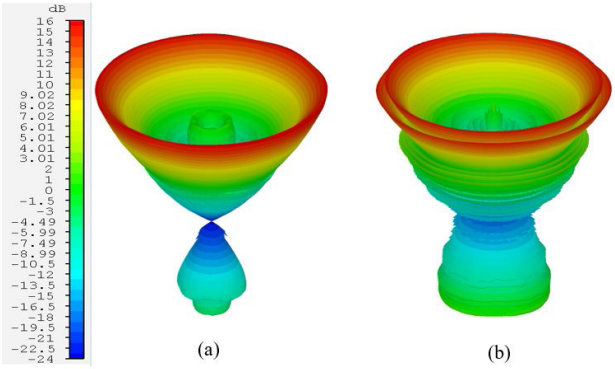

FIGURE 18. Simulated 3-D radiation patterns at 24 GHz. (a) Sum pattern. (b) Difference pattern ($\theta_t = 40°$).

Mechanically movement of the feed is shown in Fig. 19. Fig. 20 shows the SD beams of the proposed antenna for feed

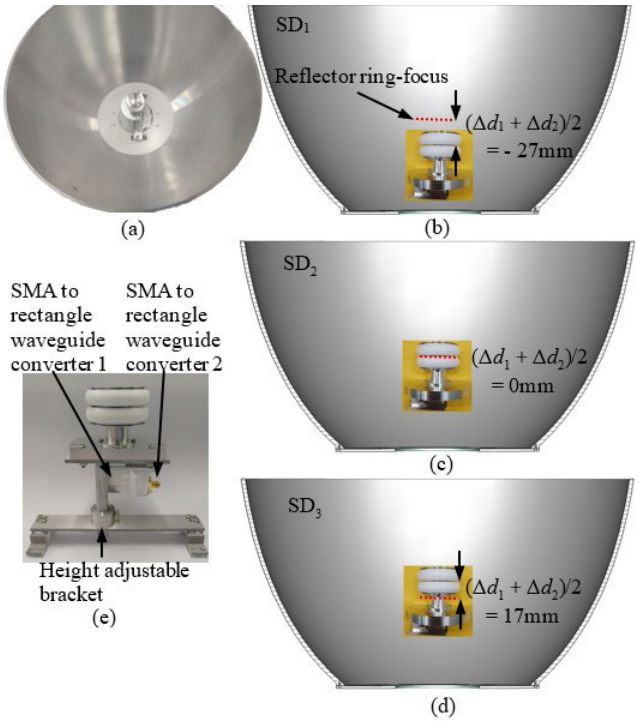

FIGURE 19. Schematic representation of a 1-D mechanically scanned. (a) Top view of the proposed SD conical beam-scanning reflector antenna. (b) Cut view of the proposed antenna, the feed moves downward by 27mm. (c) Cut view of the proposed antenna, the feed at the focus. (d) Cut view of the proposed antenna, the feed moves upward by 17mm. (e) Feed network with height adjustable bracket.

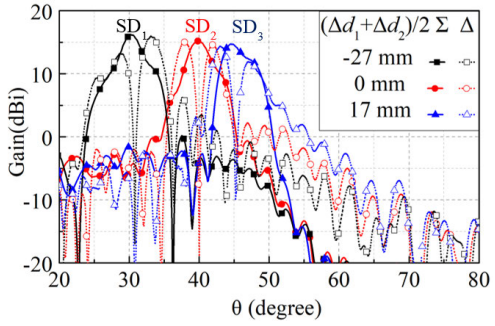

FIGURE 20. Simulation of yoz cut patterns at different positions along the symmetry axis of the proposed antenna (only half is shown because of the symmetry).

horns at different positions along the symmetry axis, which are synthesized by the corresponding conical beams shown in Fig. 16. The asymmetry of the difference beam at 30.8° and 45.2° was caused by the amplitude asymmetry and phase deviation from the patterns of the single horns.

IV. ERROR ANALYSIS ANGLE MEASUREMENT

As shown in Fig. 16, two conical beams produced by two single horns experience 4-dB crossover, when the spacing between primary-feed horns was set to 11 mm. To simplify the analysis, Gaussian function was used to fit the half part of the normalized conical beam in *yoz* plane at 40°, as described in [39]:

$$F_l = e^{-\alpha(\theta_{tgt}-\theta_l)^2}$$
$$F_r = e^{-\alpha(\theta_{tgt}-\theta_r)^2} \quad (5)$$

where θ_{tgt} is the target elevation angle, θ_{l} and θ_{r} are the beam point angles of the two conical beams $F_{\text{l}}(\theta)$ and $F_{\text{r}}(\theta)$, $F_{\text{l}}(\theta_{\text{tgt}})$ and $F_{\text{r}}(\theta_{\text{tgt}})$ are the output signal amplitudes of the two channels. θ_{4dB} is equal to the difference between θ_{l} and θ_{r}. Therefore:

$$F_l(\theta_s) = e^{-\alpha\theta_{4dB}^2/4} = \sqrt{0.4} \quad (6)$$

where θ_{s} is the angle of null-depth. Accordingly, parameter α can be obtained thus:

$$\alpha = \frac{4\ln\sqrt{2.5}}{\theta_{4dB}^2} \quad (7)$$

The monopulse error signal u can be obtained by the following [40]:

$$u_{error} = u_0\cos\beta = \frac{|F_\Delta(\theta)|}{|F_\Sigma(\theta)|}\cos\beta \quad (8)$$

where β is the phase angle between Σ and Δ beam outputs, and $\theta = \theta_{\text{tgt}} - \theta_{\text{s}}$.

The slope of the curve u_{error} is called the monopulse error slope k_{m}. It can be calculated thus:

$$k_m = \frac{du}{dx} \quad (9)$$

where $x = \theta/\theta_{\text{4dB}}$.The angular precision (standard deviation of angle error) can be calculated thus [28]:

$$\Delta\theta = \frac{\theta_{bw}}{k_m\sqrt{2SNR}}\sqrt{1+\left(\frac{k_m\theta}{\theta_{bw}}\right)^2} \quad (10)$$

where θ_{bw} is sum beam 4-dB beamwidth, and *SNR* is signal-to-noise ratio.

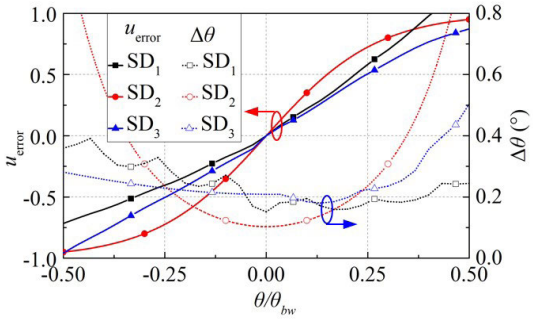

FIGURE 21. Monopulse error signal u_{error} and angle measurement accuracy $\Delta\theta$.

Accordingly, the monopulse error signal u_{error} and angle measurement accuracy $\Delta\theta$ are plotted in Fig. 21 for the case where the *SNR* is 15 dB. This error signal can be used to estimate the target's position within the Σ beam. In a tracking mode, since the angular position of the target is known, the antenna beam can be pointed directly at the target such that

the target is in the center (or at least very close to the center) of the Σ beam. As shown in Fig. 21, the maximum angle measurement accuracy $\Delta\theta$ is 0.2° at $\theta/\theta_{4dB} = 0$ in the case of beam scanning from 30.8° to 45.2°. This scanning coverage is enough to search Starlink's satellite that launched by SpaceX [41]. Besides, compared with the SD conical beam reflector antenna without scanning ability (e.g., beam point angle is only at 40°), the SD conical beam-scanning reflector antenna gives a better sum beam gain at 30.8° and 45.2°, which is more than 15dBi. Based on the above-mentioned theoretical finding, a prototype was fabricated and tested. The experimental results are presented in the next section.

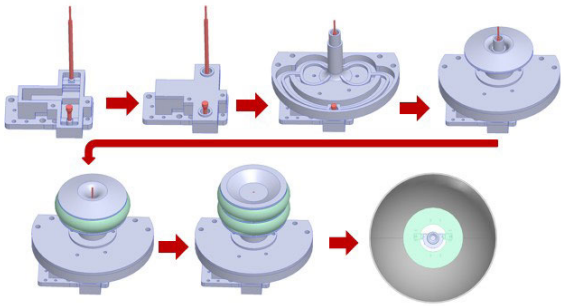

FIGURE 22. Assembly process of the proposed antenna.

V. FABRICATION AND RESULTS

The assembly process of the prototype is illustrated in Fig. 22. Fabrication of the complete feed system and reflector antenna is shown in Fig. 23. The reflection coefficients of the antenna were measured by the network analyzer Agilent E8722ES, and the radiation patterns in an anechoic chamber.

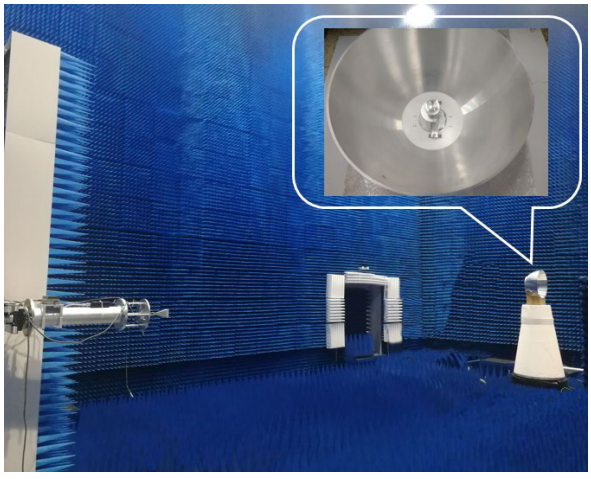

FIGURE 23. SD conical beam-scanning reflector antenna under test in an anechoic chamber.

Fig. 24 depicts the simulated and measured reflection coefficients of the fabricated SD conical beam-scanning antenna prototype. The measured –10-dB impedance bandwidth is from 22.7 to 25.4 GHz. It can be observed that simulation

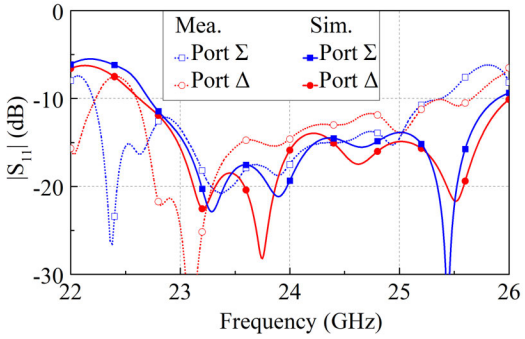

FIGURE 24. Simulated and measured reflection coefficients of the fabricated SD conical beam-scanning reflector antenna.

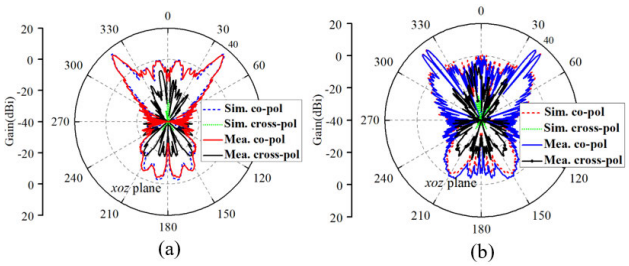

FIGURE 25. Simulated and measured xoz cut radiation patterns of the fabricated SD conical beam-scanning reflector antenna. (a) Sum pattern. (b) Difference pattern. (SD_2).

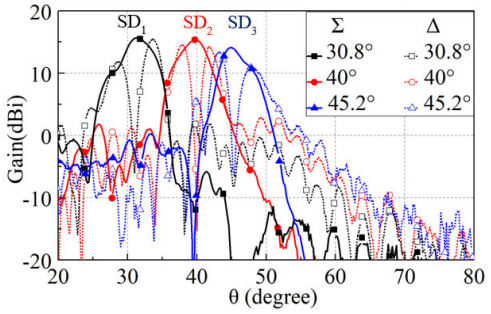

FIGURE 26. Measured scanning yoz cut radiation patterns of the fabricated SD conical beam-scanning reflector antenna (only half is shown because of the symmetry).

curves present good agreement with measurement within the band 23.5 GHz and 25 GHz. The measurement operating frequencies are lower than the simulation ones are caused by fabrication errors (e.g. positive error of l_h) and the gap created by assembly. And the measurement differences between Port Σ and Δ in Fig. 24 are due to the fabrication errors between the two converters shown in Fig. 19 (e). Fig. 25 shows the simulated and measured radiation patterns of the fabricated SD conical beam reflector antenna at 40°. It can be seen that cross-polarization levels remain below −25 dB. Low cross-polarization levels are because of the TEM mode feeding and complete symmetry. The measured radiation patterns of the designed antenna are given in Fig. 26, including three conical beam-scanning angles. The results show that the

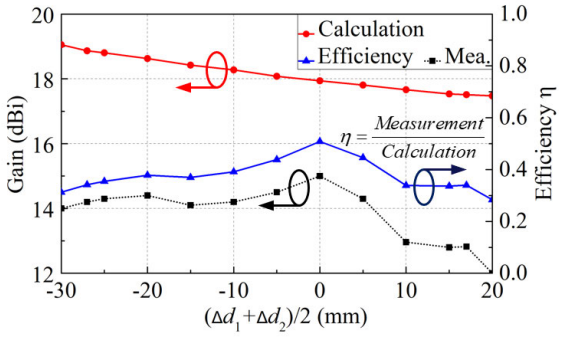

FIGURE 27. Radiation efficiency and realized gain for the proposed antenna over the scan range (The red curve is calculated by equation (2)).

sum beam gain varies by less than 1.5 dB, across the scan coverage. Fig. 27 shows the radiation efficiency and realized gain for the proposed antenna over the scan range. It can be found that whether the feed horns move upward from the reflector ring-focus or move downward, the efficiency will reduce. This is because when the feed antenna is off-focus, the spillover of the energy from the reflector increases. The measured and simulated results of the reflection coefficients and radiation patterns are found to be in good agreement, except for a small discrepancy, which might have been caused by manufacturing errors and experimental tolerance. The results show that the designed antenna can achieve high-gain SD conical beam-scanning.

VI. CONCLUSION

In this paper, a SD conical beam-scanning reflector antenna has been proposed. A compact feed network with equal-power-division, high isolation, and good phase-balance was developed for the proposed antenna. Coaxial waveguide-to-rectangular waveguide transition was designed. The reflector, which is a body of revolution illuminated by nested coaxial horns, was analyzed by geometrical optics. As a result, 11% impedance bandwidth could be achieved for the whole SD conical beam-scanning reflector antenna. Two 16-dBi conical beams were obtained and used to generate SD conical beams by a comparator network. By mechanically moving the feed horns along z axis, 30.8° to 45.2° one-dimensional tracking of the SD conical beam reflector antenna could be achieved. With the proposed antenna, accuracy of 0.2° could be achieved in measuring the SD amplitude comparison angle. A prototype of the proposed antenna was fabricated and tested. The test results demonstrate the validity of the proposed methodology. The advantages of the proposed antenna are its sum and difference conical beam-scanning, and low cost, besides the ease with which it can be fabricated and assembled. The proposed SD conical beam-scanning reflector antenna has the potential for applications in satellite communication systems.

REFERENCES

[1] S. Borisov and A. Shishlov, "Antennas for satcom-on-the-move, review," in *Proc. Int. Conf. Eng. Telecommun. (EnT)*, Nov. 2014, pp. 3–7.

[2] J. Zhao, H. Li, X. Yang, W. Mao, B. Hu, T. Li, H. Wang, Y. Zhou, and Q. Liu, "A compact Ka-band monopulse cassegrain antenna based on reflectarray elements," *IEEE Antennas Wireless Propag. Lett.*, vol. 17, no. 2, pp. 193–196, Feb. 2018.

[3] P. F. Kou and Y. J. Cheng, "A dual circular-polarized extremely thin monopulse feeder at W-band for prime focus reflector antenna," *IEEE Antennas Wireless Propag. Lett.*, vol. 18, no. 2, pp. 231–235, Feb. 2019.

[4] S. S. Roy, C. Saha, T. Nagasekhar, S. B. Mane, C. S. Padmavathy, G. Umadevi, and M. N. Kumar, "Design of a compact multielement monopulse feed for ground-station satellite tracking applications," *IEEE Antennas Wireless Propag. Lett.*, vol. 18, no. 9, pp. 1721–1725, Sep. 2019.

[5] H.-L. Peng, W.-Y. Yin, J.-F. Mao, and Y.-T. Xie, "A compact single/dual-polarized broadband antenna with SUM and difference beam capabilities," *IEEE Antennas Wireless Propag. Lett.*, vol. 9, pp. 990–993, Nov. 2010.

[6] S. Radavaram and M. Pour, "Wideband radiation reconfigurable microstrip patch antenna loaded with two inverted U-slots," *IEEE Trans. Antennas Propag.*, vol. 67, no. 3, pp. 1501–1508, Mar. 2019.

[7] C. Deng, X. Lv, and Z. Feng, "Wideband dual-mode patch antenna with compact CPW feeding network for pattern diversity application," *IEEE Trans. Antennas Propag.*, vol. 66, no. 5, pp. 2628–2633, May 2018.

[8] W. Lin, H. Wong, and R. W. Ziolkowski, "Circularly polarized antenna with reconfigurable broadside and conical beams facilitated by a mode switchable feed network," *IEEE Trans. Antennas Propag.*, vol. 66, no. 2, pp. 996–1001, Feb. 2018.

[9] X. Yang, H. Lin, H. Gu, L. Ge, and X. Zeng, "Broadband pattern diversity patch antenna with switchable feeding network," *IEEE Access*, vol. 6, pp. 69612–69619, 2018.

[10] J. Wang, X.-S. Yang, X. Ding, and B.-Z. Wang, "Topology optimization of conical-beam antennas exploiting rotational symmetry," *IEEE Trans. Antennas Propag.*, vol. 66, no. 5, pp. 2254–2261, May 2018.

[11] S. V. Kumar and A. R. Harish, "Generation of circularly polarized conical beam pattern using torus knot antenna," *IEEE Trans. Antennas Propag.*, vol. 65, no. 11, pp. 5740–5746, Nov. 2017.

[12] G. Chenhu, J. Geng, H. Zhou, J. Li, L. Liu, X. Liang, W. Zhu, R. Jin, and R. W. Ziolkowski, "Truncated circular cone slot antenna array that radiates a circularly polarized conical beam," *IEEE Antennas Wireless Propag. Lett.*, vol. 16, pp. 2574–2577, Aug. 2017.

[13] J.-S. Row and T.-Y. Lin, "Frequency-reconfigurable coplanar patch antenna with conical radiation," *IEEE Antennas Wireless Propag. Lett.*, vol. 9, pp. 1088–1091, Nov. 2010.

[14] D. Comite, V. G.-G. Buendia, S. K. Podilchak, D. D. Ruscio, P. Baccarelli, P. Burghignoli, and A. Galli, "Planar antenna design for omnidirectional conical radiation through cylindrical leaky waves," *IEEE Antennas Wireless Propag. Lett.*, vol. 17, no. 10, pp. 1837–1841, Oct. 2018.

[15] D. Hua, S.-S. Qi, W. Wu, and D.-G. Fang, "Synthesis of conical beam array antenna with concentric loop configuration using element-level pattern diversity technique," *IEEE Trans. Antennas Propag.*, vol. 66, no. 11, pp. 6397–6402, Nov. 2018.

[16] S.-S. Qi, W. Wu, and D.-G. Fang, "Dual/single band conical-beam nested horn antennas with dual/single pointing angles," *IEEE Trans. Antennas Propag.*, vol. 60, no. 10, pp. 4911–4915, Oct. 2012.

[17] Y. F. Cao and X. Y. Zhang, "Low-profile conical-pattern slot antenna with wideband performance using artificial magnetic conductors," *IEEE Trans. Antennas Propag.*, vol. 66, no. 4, pp. 1685–1694, Apr. 2018.

[18] S.-S. Qi, W. Wu, and D.-G. Fang, "High gain conical beam antenna with large beam-pointing angle by using hemitorus lens-reflector," in *Proc. 3rd Asia–Pacific Conf. Antennas Propag.*, Jul. 2014, pp. 430–432.

[19] D. Guan, Y. Zhang, Z. Qian, and J. Zhang, "Compact circular polarised SIW array antenna with high gain and conical-beam," *Electron. Lett.*, vol. 51, no. 24, pp. 1962–1964, Nov. 2015.

[20] L. Cui, S.-S. Qi, W. Wu, and D.-G. Fang, "High gain conical beam antenna array exploiting grating lobes," *IEEE Trans. Antennas Propag.*, vol. 63, no. 2, pp. 848–853, Feb. 2015.

[21] S.-H. Son, S.-I. Jeon, C.-J. Kim, and W. Hwang, "GA-based design of multi-ring arrays with omnidirectional conical beam pattern," *IEEE Trans. Antennas Propag.*, vol. 58, no. 5, pp. 1527–1535, May 2010.

[22] B. Zhou and J. Geng, "An omnidirectional circularly polarized slot array with high gain in a wide bandwith," *IEEE Antennas Wireless Propag. Lett.*, vol. 14, pp. 666–669, 2016.

[23] D. Hua, S.-S. Qi, W. Wu, and D.-G. Fang, "CPW-fed printed antenna array with conical beam," *IEEE Trans. Antennas Propag.*, vol. 64, no. 3, pp. 1096–1100, Mar. 2016.

[24] A. R. Giddis and R. B. Barrar, "An improved ground beacon antenna," *IEEE Trans. Aerosp. Navigational Electron.*, vol. ANE-10, no. 4, pp. 315–323, Dec. 1963.
[25] F. J. da Silva Moreira and J. R. Bergmann, "Axis-displaced dual-reflector antennas for omnidirectional coverage with arbitrary main-beam direction in the elevation plane," *IEEE Trans. Antennas Propag.*, vol. 54, no. 10, pp. 2854–2861, Oct. 2006.
[26] S. R. Zang and J. R. Bergmann, "Omnidirectional dual-reflector antennas for flexible coverage," *IEEE Antennas Wireless Propag. Lett.*, vol. 12, pp. 821–824, Jun. 2013.
[27] J. R. Bergmann and F. J. S. Moreira, "An omnidirectional ADE reflector antenna," *Microw. Opt. Technol. Lett.*, vol. 40, no. 3, pp. 250–254, Feb. 2004.
[28] S. M. Sherman and D. K. Barton, *Monopulse Principles and Techniques*. Norwood, MA, USA: Artech House, 2011.
[29] W. Yi, E. Li, G. Guo, and R. Nie, "An X-band coaxial-to-rectangular waveguide transition," in *Proc. IEEE Int. Conf. Microw. Technol. Comput. Electromagn.*, May 2011, pp. 129–131.
[30] J. R. Montejo-Garai, J. A. Ruiz-Cruz, and J. M. Rebollar, "Design of a Ku-band high-purity transducer for the TM_{01} circular waveguide mode by means of T-type junctions," *IEEE Access*, vol. 7, pp. 450–456, 2019, doi: 10.1109/ACCESS.2018.2885489.
[31] K. W. Kark and R. Dill, "A general theory on the graphical representation of antenna-radiation fields," *IEEE Trans. Antennas Propag.*, vol. 38, no. 2, pp. 160–165, Feb. 1990.
[32] I. Göngör, and A. Ünal, "Design of a vertically polarized omnidirectional antenna at Ka-band," in *Proc. IEEE Int. Symp. Antennas Propag. (APSURSI)*, Fajardo, Puerto Rico, Oct. 2016, pp. 129–130.
[33] A. Rudge, "Multiple-beam antennas: Offset reflectors with offset feeds," *IEEE Trans. Antennas Propag.*, vol. AP-23, no. 3, pp. 317–322, May 1975.
[34] S. Sandler, "Paraboloidal reflector patterns for off-axis feed," *IRE Trans. Antennas Propag.*, vol. 8, no. 4, pp. 368–379, Jul. 1960.
[35] A. W. Rudge and M. J. Withers, "New technique for beam steering with fixed parabolic reflectors," *Proc. Inst. Electr. Eng.*, vol. 118, no. 7, pp. 857–863, Jul. 1971.
[36] A. Mrstik, "Scan limits of off-axis fed parabolic reflectors," *IEEE Trans. Antennas Propag.*, vol. AP-27, no. 5, pp. 647–651, Sep. 1979.
[37] J. Ruze, "Lateral-feed displacement in a paraboloid," *IEEE Trans. Antennas Propag.*, vol. AP-13, no. 5, pp. 660–665, Sep. 1965.
[38] Y. Lo, "On the beam deviation factor of a parabolic reflector," *IRE Trans. Antennas Propag.*, vol. 8, no. 3, pp. 347–349, May 1960.
[39] Q. He, Z. He, and H. Li, "Multibeam amplitude comparison problems for MIMO radar's angle measurement," in *Proc. IEEE Signals, Syst. Comput.*, Pacific Grove, CA, USA, Nov. 2007, pp. 2163–2167.
[40] M. A. Richards, J. A. Scheer, and W. A. Holm, "Principles of modern radar," in *Basic Principles*, vol. 1. Rijeka, Croatia: SciTech, 2010.
[41] A. Sayin, M. Cherniakov, and M. Antoniou, "Passive radar using starlink transmissions: A theoretical study," in *Proc. 20th Int. Radar Symp. (IRS)*, Ulm, Jun. 2019, pp. 1–7.

JUNXIANG YANG (Student Member, IEEE) was born in Xihua, Henan, China, in 1992. He received the B.Eng. degree in new energy science and engineering from the Nanjing University of Science and Technology (NUST), Nanjing, China, in 2015, where he is currently pursuing the Ph.D. degree in electromagnetic field and microwave technology.

His current research interests include conical beam antenna, helix antenna, and reflector antenna.

SHI-SHAN QI (Member, IEEE) was born in Shandong, China, in 1983. He received the B.S. degree in electronic information engineering and the Ph.D. degree in communications and information systems from the Nanjing University of Science and Technology, Nanjing, China, in 2005 and 2012, respectively.

Since 2016, he has been an Associate Professor with the School of Electronic and Optical Engineering, Nanjing University of Science and Technology. His current research interests include conical beam antenna, reconfigurable water antennas, wireless power transmission, and microwave- and millimeter-wave theories and technologies.

WEN WU (Senior Member, IEEE) received the Ph.D. degree in electromagnetic field and microwave technology from Southeast University, Nanjing, China, in 1997.

He is currently a Professor with the School of Electronic Engineering and Optoelectronic Technology, Nanjing University of Science and Technology, Nanjing, where he is also an Associate Director of the Ministerial Key Laboratory, JGMT. He has authored or coauthored over 60 journal articles and conference papers. He has submitted five patent applications. His current research interests include microwave and millimeter-wave theories and technologies, microwave and millimeter-wave detection, and multimode compound detection.

Dr. Wu was a recipient of six times of the Ministerial and Provincial-Level Science and Technology Awards.

DA-GANG FANG (Life Fellow, IEEE) was born in Shanghai, China. He graduated from the Graduate School of Beijing Institute of Posts and Telecommunications, Beijing, China, in 1966.

From 1980 to 1982, he was a Visiting Scholar with Laval University, Quebec, QC, Canada, and with the University of Waterloo, Waterloo, ON, Canada. Since 1986, he has been a Professor with the Nanjing University of Science and Technology, Nanjing, China. His current research interests include computational electromagnetics and microwave integrated circuits and antennas.

Prof. Fang is a Fellow of the Chinese Institute of Electronics (CIE). He was a member of the International Advisory Committee of several international conferences. He was a recipient of the certificates from the IEEE TRANSACTIONS ON ANTENNAS AND PROPAGATION for his exceptional performance as a Reviewer twice, from 2014 to 2015 and from 2016 to 2017, the National Outstanding Teacher Award, the People's Teacher Medal, and the Provincial Outstanding Teacher Award. He was a TPC Chair of ICMC 1992, the Vice-General Chair of PIERS 2004, a TPC Co-Chair of APMC 2005, the General Co-Chair of ICMMT 2008, and an International Advisory Committee Co-Chair of iWEN 2016.